

Zeros of Green Functions in Topological Insulators

Takahiro Misawa^{1,2,3} and Youhei Yamaji⁴

¹ *Beijing Academy of Quantum Information Sciences, Haidian District, Beijing 100193, China*

² *Research Institute for Science and Engineering, Waseda University,
3-4-1, Okubo, Shinjuku, Tokyo 169-8555, Japan*

³ *Institute for Solid State Physics, University of Tokyo,
5-1-5 Kashiwanoha, Kashiwa, Chiba 277-8581, Japan and*

⁴ *Department of Applied Physics, University of Tokyo,
7-3-1 Hongo, Bunkyo-ku, Tokyo 113-8656, Japan*

(Dated: February 28, 2025)

This study demonstrates that the zeros of the diagonal components of Green functions are key quantities that can detect topological nature of insulators. We show that the crosses of the zeros of Green functions universally appear in all six classes of conventional topological insulators. The present study proves that the existence of the crosses of the zeros in the bulk Green functions are guaranteed because of gapless edge states. The relevance of the zeros for detecting the exotic topological insulators such as the higher-order topological insulators is also discussed. The analysis demonstrates that the zeros can be used to detect gapless surface/edge states and thus useful for searching topological materials.

I. INTRODUCTION

The Green function is one of the most fundamental tools used for solving quantum many-body problems^{1,2}. The Green function method can be used to perform a systematic analysis for a wide range of quantum many-body systems, from elementary particle physics to condensed matter physics. One of the key components of the Green function is the pole, at which the value of the Green function becomes infinite. In solid state physics, the poles correspond to band dispersion in solids and play a central role in describing the low-energy excitations of solids.

In insulating phases, the zeros of the Green function, rather than the poles, appear in the bandgap. The zeros can be used for characterizing the insulating phases, wherein the poles (band dispersions) do not govern low-energy physics. In fact, it has been proposed that the surface of the zeros of Green functions (zeros' surfaces) in Mott insulators can act as Fermi surfaces in metallic phases³. For particle-hole symmetric systems, it has been demonstrated that the Luttinger's sum rules on the zeros' surface can be satisfied for the insulating phases⁴. Moreover, studies on the doped Mott insulators have established that the interplay of the zeros and poles of the Green functions can govern the unconventional electronic properties such as non-Fermi liquid behaviors, pseudogap phenomena, and Fermi arc structures that are observed in high- T_c cuprates^{5,6}.

Recent findings on topological insulators⁷ have triggered intensive experimental and theoretical investigations of topological materials⁸⁻¹¹. Systematic clarifications of topological insulators have been proposed¹¹⁻¹³, and the periodic table for six conventional classes of topological insulators has been established, as presented in Table I. It has also been demonstrated that the existence of the topological invariant is related with the gapless surface states¹⁴.

class	Θ	Ξ	Γ	$d = 1$	2	3	4
A	0	0	0	0	\mathbb{Z}	0	\mathbb{Z}
AI	1	0	0	0	0	0	$2\mathbb{Z}$
AII	-1	0	0	0	\mathbb{Z}_2	\mathbb{Z}_2	\mathbb{Z}
AIII	0	0	1	\mathbb{Z}	0	\mathbb{Z}	0
BDI	-1	-1	1	\mathbb{Z}	0	0	0
CII	1	1	1	$2\mathbb{Z}$	0	\mathbb{Z}_2	\mathbb{Z}_2

TABLE I: Periodic table of topological insulators under four dimensions¹². The indices Θ , Ξ , and Γ represent the time-reversal symmetry, particle-hole symmetry, and chiral symmetry. For topological insulators without chiral symmetry ($\Gamma = 0$, upper panel), this study demonstrates that the zeros of the Green function cross in the bandgap. For topological insulators with chiral symmetry ($\Gamma = 1$, lower panel), this investigation establishes that it is necessary to perform an appropriate unitary transformation to observe the cross of the zeros.

Although topological insulators can be detected by calculating the topological invariants, direct calculations of the topological invariants are generally not easy. Thus, several simplified methods have been proposed for detecting the topological phases, such as the Fu-Kane formula¹⁵ for the \mathbb{Z}_2 topological insulators with the inversion symmetry. Recently, a method that uses symmetry indicators was proposed¹⁶, and it has been applied to a wide range of topological materials¹⁷⁻²².

The present study shows that the zeros of the Green functions are useful quantities for detecting the topological insulators. Because the microscopic Hamiltonians for the topological insulators are generally multi-orbital systems, we should consider the matrices of the Green functions. This investigation focuses on the zeros of the diagonal component of the Green functions because they have characteristic features. These zeros exist between poles and are given by the eigenvalues of the minor matrix M_n , which is obtained by removing the n th row and column from the original Hamiltonian. It is noted that the sim-

ple and fundamental relationship between the zeros of the Green functions and the minor matrix is not well known. This study proves that these characteristic features are obtained from an argument that is provided in Ref. [23], which rediscovers the fundamental but lesser-known identity between the eigenvectors and the eigenvalues called the *eigenvalue-eigenvector identity*. The fact that the eigenvalue-eigenvector identity is not widely known may be the main reason why the relationship between the zeros and the minor matrix is not well understood. The relationship with the minor matrix offers a mathematical foundation that can be used to analyze the zeros of the Green functions. It also offers an efficient way to numerically obtain the zeros of the Green functions, i.e., it is *not* necessary to search for the zeros in the energy direction.

By using the mathematical foundation of the zeros for the diagonal component of the Green functions, we clarify their behavior in topological insulators. First, by taking the two-dimensional Chern insulator as an example (class A topological insulator in Table I), it is demonstrated that the cross of the zeros in the bulk Green functions in the bandgap can occur in topological insulators; however, there is no cross of the zeros in trivial insulators. We establish that the existence of the topological invariant (Chern number) guarantees the cross of the zeros in the bulk systems. Furthermore, it is also demonstrated that the gapless edge states inevitably induce the crosses of the zeros in the bulk systems. In other words, the information of the edge states is encoded in the zeros of the bulk Green functions. We call this relation the *zero-edge correspondence* (ZEC) because this offers another point of view of the bulk-edge correspondence²⁴.

It is also demonstrated that the cross of the zeros generically occurs in the other topological insulators such as the \mathbb{Z}_2 topological insulator in two and three dimensions (class AII topological insulators in Table I) as well as in $2\mathbb{Z}$ topological insulators in four dimensions (class AI topological insulators in Table I). This study also investigates the zeros in topological insulators with chiral symmetry (lower panel in Table I) and shows that crosses of the zeros also occur in chiral topological insulators when we take appropriate gauges that make the Hamiltonians *not* block off-diagonal form.

Recent studies have suggested the existence of exotic topological phases, which are not listed in Table I. Higher-order topological insulators^{25,26}, which show hinge states or quantized corner charges, are candidates for these exotic topological phases. This study demonstrates that the zeros of Green functions are also useful for detecting higher-order topological insulators. These results indicate that the cross of the zeros is a universal feature of the topological phases.

Although the importance of the zeros of the Green functions for the interacting topological insulators has been proposed by Gurarie in Ref. [27], the definition of the zeros of the Green functions for the present study is different from the definition used in Ref. [27]. Because

Gurarie's argument is based on the *diagonalized* Green functions, which have no zeros in the non-interacting case, this method cannot be applied to non-interacting topological insulators. In contrast, our argument is based on the diagonal components of the Green functions that can characterize the non-interacting topological insulators as well as interacting ones, as will be described in detail below. It is noted that the diagonalized Green function at the zero frequency^{28,29} is used for detecting the interacting topological phases.

This paper is organized as follows. In Sec. II, the mathematical foundation of the zeros of the diagonal components of the Green functions is explained. In Sec. III, we examine the zeros of the Green function for two-dimensional Chern insulators and demonstrate that the crossing of the zeroes is induced by the non-trivial Chern number. We also demonstrate that the crossing of the zeroes is gauge invariant and it is induced by the gapless edge state.

Sec. IV establishes that the crosses of the zeros occur in \mathbb{Z}_2 topological insulators in two and three dimensions. We also give an intuitive argument for the crosses of the zeros in the topological insulators. In Sec. V, we examine the zeros in topological insulators with chiral symmetry and demonstrate that it is necessary to use appropriate gauges of the Hamiltonian to see the crosses of the zeros in the topological phases. Sec. VI shows that the crosses of the zeros occur even for higher-order topological insulators. Finally, Sec. VII summarizes the study.

II. MATHEMATICAL FOUNDATION OF ZEROS OF THE GREEN FUNCTION

In this section, we discuss the mathematical foundation of the zeros of the diagonal components of Green functions. By following the argument in Ref. [23], we show that the zeros can be represented by the eigenvalues of the minor matrix M_n of the Hamiltonian H , which is generated by removing the n th row and column from H .

Using the eigenvalues and eigenvectors of the Hamiltonian $H(\mathbf{k})$, where (\mathbf{k}) represents the momentum, the n th diagonal component of the Green function is expressed as

$$G_n(\mathbf{k}, \omega) = (\omega I - H(\mathbf{k}))_{nn}^{-1} = \sum_{i=1}^N \frac{|\Psi_i^{(n)}(\mathbf{k})|^2}{\omega - E_i(\mathbf{k})}, \quad (1)$$

$$H(\mathbf{k})\Psi_i(\mathbf{k}) = E_i(\mathbf{k})\Psi_i(\mathbf{k}). \quad (2)$$

where $E_i(\mathbf{k})$ is the i th eigenvalue of the Hamiltonian and $\Psi_i^{(n)}(\mathbf{k})$ is the n th component of the i th eigenvector.

for $\Psi_i(\mathbf{k})$. By applying the Cramer's rule, we can obtain

$$G_n(\mathbf{k}, \omega) = \sum_{i=1}^N \frac{|\Psi_i^{(n)}(\mathbf{k})|^2}{\omega - E_i(\mathbf{k})} = \frac{\det(\omega I_{N-1} - M_n(\mathbf{k}))}{\det(\omega I_N - H(\mathbf{k}))} = \frac{\prod_{l=1}^{N-1} [\omega - E_l(M_n(\mathbf{k}))]}{\prod_{l=1}^N [\omega - E_l(H(\mathbf{k}))]}, \quad (3)$$

where I_N represents the N -dimensional identity matrix. This relation Eq. (3) shows that the zeros of $G_n(\mathbf{k}, \omega)$ are represented by the eigenvalues of M_n . It is known that the eigenvalues of the minor matrix M_n exist between the eigenvalues of the original Hamiltonian H , i.e.,

$$E_i(H) \leq E_i(M_n) \leq E_{i+1}(H). \quad (4)$$

The above relation is known as the Cauchy interlacing inequalities relation^{30,31}. A proof of the inequalities is given in Appendix A.

By applying the residue theorem to Eq. (3), the following expression can be obtained.

$$|\Psi_i^{(n)}(\mathbf{k})|^2 = \frac{\prod_{l=1}^{N-1} [E_i(H(\mathbf{k})) - E_l(M_n(\mathbf{k}))]}{\prod_{l=1, l \neq i}^N [E_i(H(\mathbf{k})) - E_l(H(\mathbf{k}))]}. \quad (5)$$

This relation Eq. (5) is called the *eigenvector-eigenvalue identity* and has been recently rediscovered²³. From this identity, it can be concluded that the zero and the pole should coincide if the n th component of the eigenvectors become zero and vice versa.

III. TWO-DIMENSIONAL CHERN INSULATOR (CLASS A)

A. Zeros and poles in the Chern insulator

To examine the behaviors of the zeros of the Green functions in topological insulators, we employed a two-band model for a two-dimensional Chern insulator³² on a square lattice, defined as follows.

$$H_A = \sum_{\nu=x,y} H_\nu + H_{\text{diag}}, \quad (6)$$

$$H_\nu = \sum_j h_{\nu,j}, \quad (7)$$

$$h_{\nu,j} = c_{j+\mathbf{e}_\nu}^\dagger T_\nu c_j + \text{H.c.}, \quad (8)$$

$$H_{\text{diag}} = (2+m) \sum_j c_j^\dagger \sigma_z c_j, \quad (9)$$

where c_j^\dagger (c_j) represents the two-component fermion creation (annihilation) operator that is defined on the site j on the square lattice spanned by two orthogonal unit vectors $\mathbf{e}_{\nu=x,y}$. The matrices T_ν are defined as

$$T_x = (-\sigma_z + i\sigma_x)/2, \quad (10)$$

$$T_y = (-\sigma_z + i\sigma_y)/2, \quad (11)$$

$$(12)$$

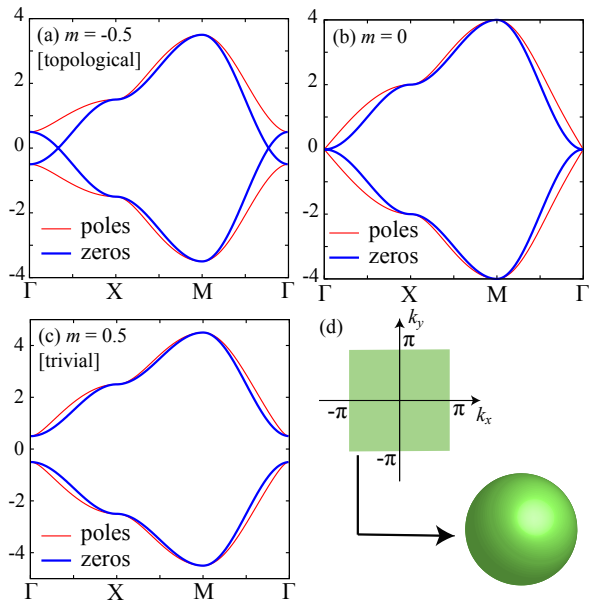


FIG. 1: (a)-(c) Band dispersions (thin red lines) and zeros (thick blue lines) of the diagonal Green functions in the Hamiltonians defined in Eq. (9). For $-4 < m < 0$, the system becomes a topological insulator (Chern insulator) while it becomes a trivial band insulator for $m > 0$. At $m = 0$, the quantum phase transition between the topological insulator and the trivial band insulator can occur ($m > 0$). The zeros of the Green functions cross each other in the topological insulator while they do not cross in the trivial band insulator. (d) Brillouin zone and two-dimensional sphere. In the topological insulator with the Chern number 1, there is a one-to-one mapping from the Brillouin zone to the two-dimensional sphere.

where

$$\sigma_x = \begin{pmatrix} 0 & 1 \\ 1 & 0 \end{pmatrix}, \sigma_y = \begin{pmatrix} 0 & -i \\ i & 0 \end{pmatrix}, \sigma_z = \begin{pmatrix} 1 & 0 \\ 0 & -1 \end{pmatrix}. \quad (13)$$

It is noted that the system becomes a topological (Chern) insulator for $-4 < m < 0$, and it becomes a trivial band insulator for $m > 0$.

The Hamiltonian in the momentum space can be described as

$$H_A(\mathbf{k}) = \begin{pmatrix} R_z(\mathbf{k}) & R_x(\mathbf{k}) - iR_y(\mathbf{k}) \\ R_x(\mathbf{k}) + iR_y(\mathbf{k}) & -R_z(\mathbf{k}) \end{pmatrix}, \quad (14)$$

$$R_x(\mathbf{k}) = \sin k_x, \quad (15)$$

$$R_y(\mathbf{k}) = \sin k_y, \quad (16)$$

$$R_z(\mathbf{k}) = 2 + m - (\cos k_x + \cos k_y). \quad (17)$$

By diagonalizing the Hamiltonian, the eigenvalues (band dispersions) can be obtained as

$$E_{\pm}(\mathbf{k}) = \pm |R(\mathbf{k})| = \sqrt{R_x(\mathbf{k})^2 + R_y(\mathbf{k})^2 + R_z(\mathbf{k})^2}. \quad (18)$$

Following the argument in Sec. II, the zeros of the Green functions are represented by the eigenvalues of the minor matrix M_n . For the 2×2 matrices, the eigenvalues are the diagonal components of the Hamiltonian. Thus, the zeros of the n th diagonal component of the Green function (ζ_n) are represented by

$$\zeta_0(\mathbf{k}) = M_0(\mathbf{k}) = -R_z(\mathbf{k}), \quad (19)$$

$$\zeta_1(\mathbf{k}) = M_1(\mathbf{k}) = R_z(\mathbf{k}). \quad (20)$$

In Fig. 1(a)-(c), a plot is presented for the band dispersions and zeros of the Green functions for several values of m . It was observed that the zeros of the Green function cross each other in the topological insulator while they do not cross in the trivial insulator. This feature of the zeros is in sharp contrast with the band dispersions (poles of Green functions). This is because it is impossible to distinguish the topological insulator and band insulator based on only the band dispersions. When considering the standard way to identify the topological insulators, it is necessary to examine the existence of the topological invariant or the gapless edge states. However, as shown in Fig. 1, the cross of the zeros of the Green functions in the bulk system can be used to identify the topological insulator. The next subsection explains how the topological invariant can guarantee the cross of the zeros of the Green functions.

B. Relation with the Chern number

This subsection shows that the topological invariance (Chern number \mathcal{C}) guarantees the cross of the zeros in the bandgap. From the eigenvector-eigenvalue identity Eq. (5), an important relation can be obtained: a component of the eigenvector is zero ($|\Psi_j^{(n)}(\mathbf{k})|^2 = 0$) \leftrightarrow the zeros and poles of the Green function coincide ($\zeta(\mathbf{k}) = E(\mathbf{k})$). These special points where $|\Psi_j^{(n)}|^2 = 0$ are called the cores of the vorticity³³. From the existence of such a special point, it is demonstrated how the topological invariant guarantees the cross of the zeros. If the Chern number \mathcal{C} is nontrivial, for example, $\mathcal{C} = 1$, there is a one-to-one mapping from $(R_x(\mathbf{k}), R_y(\mathbf{k}), R_z(\mathbf{k}))$ to the two-dimensional sphere S^2 .

Therefore, the points in the Brillouin zone exist where $(R_x(\mathbf{k}), R_y(\mathbf{k}), R_z(\mathbf{k})) \propto (0, 0, \pm 1)$. The zeros and poles coincide at these points. These points are located at $\Gamma = (0, 0)$, $X = (\pi, 0)$, and $M = (\pi, \pi)$. For $R_z = 1$ ($R_z = -1$), $\zeta_0 = E_1$, and $\zeta_1 = E_0$ ($\zeta_0 = E_0$, and $\zeta_1 = E_1$) occur. Thus, if R_z takes ± 1 (this is guaranteed by the existence of the topological invariant), ζ_0 cross with ζ_1 at least once. Therefore, the existence of the Chern number induces the cross of the zeros in the topological insulator.

In contrast to the case of the topological insulator, when the Chern number \mathcal{C} is trivial ($\mathcal{C} = 0$), there exists $(R_x(\mathbf{k}), R_y(\mathbf{k}), R_z(\mathbf{k}))$ that does not completely cover the two-dimensional sphere S^2 . In other words, one such point is present where $(R_x, R_y, R_z) \propto (0, 0, \pm 1)$ does not

exist in general. In general, the zeros of the Green function do not traverse the bandgap and do not cross. It is noted that the accidental crosses of the zeroes of the Green function might occur even in trivial insulators. An example is provided in Sec. VB.

C. Gauge invariance

As demonstrated, the cross of the zeros is guaranteed by the existence of the non-trivial topological invariant. This result indicates that the existence of the cross is gauge invariant. In this subsection, by explicitly performing the unitary transformation, it is established that the cross of the zeros is gauge invariant.

By using the unitary matrix U , a unitary transformation is performed as follows.

$$\tilde{H}(\mathbf{k}) = U^\dagger H(\mathbf{k})U, \quad (21)$$

$$U = \begin{pmatrix} u & -v \\ v^* & u \end{pmatrix} \quad (22)$$

where u is a real number, $v = v_x + iv_y$, and $u^2 + v_x^2 + v_y^2 = 1$. The explicit form of the transformed Hamiltonian is given as

$$\tilde{H}(\mathbf{k}) = \begin{pmatrix} aR_x + bR_y + cR_z & h_{\text{off}} \\ h_{\text{off}}^* & -(aR_x + bR_y + cR_z) \end{pmatrix}, \quad (23)$$

where $a = 2uv_x$, $b = -2uv_y$, $c = u^2 - v_x^2 - v_y^2$, and $h_{\text{off}} = (u^2 - v^2)R_x - i(u^2 + v^2)R_y + 2u(-iv_x + v_y)R_z$. It is noted that $a^2 + b^2 + c^2 = 1$ is satisfied. After the unitary transformation, the zeros of the Green function are given as

$$\zeta_0(\mathbf{k}) = -(aR_x(\mathbf{k}) + bR_y(\mathbf{k}) + cR_z(\mathbf{k})) \quad (24)$$

$$\zeta_1(\mathbf{k}) = (aR_x(\mathbf{k}) + bR_y(\mathbf{k}) + cR_z(\mathbf{k})). \quad (25)$$

For $R_x(\mathbf{k}) = a|R|$, $R_y(\mathbf{k}) = b|R|$, $R_z(\mathbf{k}) = c|R|$, the point where the zeros and poles coincide is given as $\zeta_0 = E_1$ and $\zeta_1 = E_0$. For the antipodal point ($R_x = -a|R|$, $R_y = -b|R|$, $R_z = -c|R|$), the point is given by $\zeta_1 = E_0$ and $\zeta_0 = E_1$. Because the existence of the topological invariant guarantees that $\mathbf{R}/|R|$ can cover the unit sphere, \mathbf{R} can take $R_x = a|R|$, $R_y = b|R|$, $R_z = c|R|$ and the corresponding antipodal point. Thus, the cross of the zeros of the Green function in Chern insulators is gauge invariant. This is consistent with the fact that the gapless edge states, which are gauge invariant, induce the crosses of the zeros, as described in Sec. III D.

D. Relation with edge states: Zero-edge correspondence

The cross of the zeros resembles the gapless edge modes, which appear in the topological insulators. This

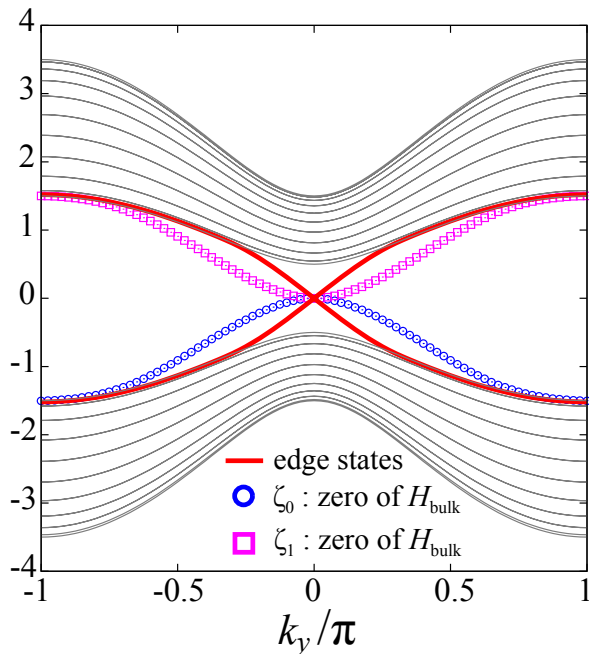


FIG. 2: Band dispersions (thin black curves) and zeros of the Green functions (blue circles and magenta squares) for the bulk Hamiltonian $H_{\text{bulk}}(L)$. For this investigation, $L = 20$ and $m = -0.5$. The zeros of the Green function are plotted in the bandgap. It is also established that the eigenvalues (thick red curves) of $H_{\text{edge}}(L-1)$ are in the bandgap. As described in the main text, the cross of the eigenvalues of $H_{\text{edge}}(L-1)$ induces the cross of the zeros in the bulk system.

subsection shows that the cross of the zeros of the Green functions has a direct relation with the gapless edge state, i.e., crosses of the eigenvalues of the edge Hamiltonian induce the cross of the zeros in the bulk Hamiltonian.

To see this, consider the Hamiltonians in the real-space configuration for the x direction (the length is set to L), which are given by

$$H_L(p) = \begin{pmatrix} h_0 & h_x & 0 & \dots & 0 & p \times h_x \\ h_{-x} & h_0 & h_x & 0 & 0 & 0 \\ 0 & h_{-x} & h_0 & h_x & 0 & 0 \\ \vdots & \vdots & \ddots & \ddots & \ddots & \vdots \\ 0 & 0 & 0 & h_{-x} & h_0 & h_x \\ p \times h_{-x} & 0 & 0 & 0 & h_{-x} & h_0 \end{pmatrix}, \quad (26)$$

$$h_0 = \begin{pmatrix} 2 + m - \cos k_y & -i \sin k_y \\ i \sin k_y & -(2 + m) + \cos k_y \end{pmatrix}, \quad (27)$$

$$h_x = \begin{pmatrix} 1/2 & i/2 \\ i/2 & -1/2 \end{pmatrix}, \quad (28)$$

$$h_{-x} = \begin{pmatrix} 1/2 & -i/2 \\ -i/2 & -1/2 \end{pmatrix}. \quad (29)$$

It is noted that the open-boundary condition corresponds to $p = 0$, and the periodic-boundary condition corre-

sponds to $p = 1$. The bulk Hamiltonian ($p = 1$) includes the $L - 1$ edge Hamiltonian

$$H_L(p = 1) = \begin{pmatrix} h_0 & B \\ B^\dagger & H_{L-1}(p = 0) \end{pmatrix}, \quad (30)$$

where $B = (h_x, 0, \dots, 0, p \times h_x)$.

The zeros of the bulk Hamiltonian ($H_L(p = 1) = H_{\text{bulk}}$) are given by the eigenvalues of the minor matrix M_n . Based on the periodicity, we only considered the eigenvalues of M_0 and M_1 . Because M_0 and M_1 include the edge Hamiltonian $H_{L-1}(p = 0) = H_{\text{edge}}$, H_{edge} can be regarded as a minor matrix of M_0 and M_1 . Thus, from the Cauchy interlacing identity, the eigenvalues of H_{edge} are located between the eigenvalues of M_0 and M_1 and vice versa. This relation can be expressed as

$$\begin{aligned} E_{i-1}(H_{\text{edge}}) &\leq E_i(M_0) = \zeta_0(H_{\text{bulk}}) \leq E_i(H_{\text{edge}}), \\ E_{i-1}(H_{\text{edge}}) &\leq E_i(M_1) = \zeta_1(H_{\text{bulk}}) \leq E_i(H_{\text{edge}}). \end{aligned} \quad (31)$$

If the eigenvalues of the edge Hamiltonian are doubly degenerate, the zeros of the bulk Hamiltonian should coincide, i.e.,

$$\zeta_0(H_{\text{bulk}}) = \zeta_1(H_{\text{bulk}}). \quad (32)$$

This indicates that the gapless edge states (they cross in the bandgap) inevitably induce the cross of the zeros in the bulk systems.

Using numerical calculations, we demonstrate the application of this argument to Chern insulators. In Fig. 2, the poles of the zeros of the Green functions for the bulk Hamiltonian $H_{L=20}(p = 1)$ are defined in Eq. (26) for $m = -0.5$. We also show the poles of the edge Hamiltonian (edge states) for $H_{L=19}(p = 0)$. We can confirm that the zeros of the bulk Hamiltonian exist between the poles of the edge Hamiltonian, and they cross when the poles of the edge Hamiltonian cross ($k_y = 0$). This result indicates that the cross of the zeros in the bulk systems is induced by the gapless edge states.

In general, for the m -orbital system (the sizes of h_x and h_0 are $m \times m$), it is demonstrated that the m -fold degeneracy in the edge states (gapless edge states) induce the m -fold degeneracy (cross) of the zeros of the bulk Hamiltonian in Appendix B. Therefore, the gapless edge/surface states inevitably induce the cross of the zeros in the bulk systems. This relation is called the *zero-edge correspondence* (ZEC). This correspondence is another point of view of the bulk-edge correspondence²⁴ since the information of the edge states can be obtained based on in the bulk properties.

Here, the ZEC and its contraposition are summarized as follows:

ZEC: m -fold degeneracy in the edge states \rightarrow m -fold degeneracy (cross) in the zeros of the bulk Green functions

Contraposition of ZEC: No cross in the zeros of the bulk Green functions \rightarrow No degeneracy in edge states

This result shows that when there is no cross of the zeros, system is not topological, and it has no gapless edge states. It can also be noted that the converse of the ZEC does *not* hold, which is shown as follows:

Converse of ZEC: m -fold degeneracy (cross) in the zeros of the bulk Green functions \rightarrow m -fold degeneracy in the edge states

As demonstrated in Sec. VB, a counter-example of the converse of the ZEC in the systems for the CII topological insulator can be identified.

IV. \mathbb{Z}_2 TOPOLOGICAL INSULATOR IN TWO AND THREE DIMENSIONS (CLASS AII)

In the previous section, as a canonical example of the topological insulators, the zeros of the Green functions in the Chern insulators were analyzed. In this section, we examine the zeros of the Green functions in the \mathbb{Z}_2 (class AII) topological insulators in two and three dimensions. It can be confirmed that the zeros cross in the bandgap in topological phases, as demonstrated in the case of the Chern insulators.

A. Kane-Mele model

As an example of the \mathbb{Z}_2 topological insulators, the Kane-Mele model⁷ was employed on the honeycomb lattice, which is defined as

$$H_{\text{KM}} = t \sum_{\langle i,j \rangle} c_i^\dagger c_j + i\lambda_{\text{SO}} \sum_{\langle\langle i,j \rangle\rangle} \nu_{ij} c_i^\dagger \sigma^z c_j + \sum_i \Delta_i c_i^\dagger c_i + i\lambda_R \sum_{\langle i,j \rangle} c_i^\dagger (\boldsymbol{\sigma} \times \mathbf{d}_{ij})_z c_j$$

where $c_i^\dagger = (c_{i\uparrow}^\dagger, c_{i\downarrow}^\dagger)$ and $c_{i\sigma}^\dagger$ ($c_{i\sigma}$) is a creation (annihilation) operator of an electron with the spin σ on site i . Each parameter is defined as follows: t represents the nearest-neighbor hopping, λ_{SO} represents the spin-orbit coupling, Δ_i is the staggered charge potential, and λ_R represents the Rashba term. $\boldsymbol{\sigma}$ is defined as $\boldsymbol{\sigma} = (\sigma^x, \sigma^y, \sigma^z)^t$ where σ^x , σ^y , and σ^z are Pauli matrices. ν_{ij} is defined as $\nu_{ij} = (\mathbf{d}_{ik} \times \mathbf{d}_{kj})_z / |\mathbf{d}_{ik} \times \mathbf{d}_{kj}|$, where \mathbf{d}_{ij} denotes the vector along two bonds that the electron traverses from site j to i through k (see Fig. 3(a)). For simplicity, we can first assume that the Rashba term is absent ($\lambda_R = 0$). The effects of the Rashba term are examined in the next subsection. For simplicity, $t = 1$.

By performing a Fourier transformation, the Hamiltonian without the Rashba terms in the momentum space

can be described as

$$H_\sigma(\mathbf{k}) = \begin{pmatrix} R_{z,\sigma}(\mathbf{k}) & R_x(\mathbf{k}) - iR_y(\mathbf{k}) \\ R_x(\mathbf{k}) + iR_y(\mathbf{k}) & -R_{z,\sigma}(\mathbf{k}) \end{pmatrix},$$

where $R_{z,\sigma}(\mathbf{k}) = \sigma E(\mathbf{k}) + \Delta$ and $E(\mathbf{k}) = 4\lambda_{\text{SO}} \sin(k_x/2)[\cos(k_x/2) - \cos(\sqrt{3}k_y/2)]$. $R_x(\mathbf{k})$ [$R_y(\mathbf{k})$] is defined as $R_x(\mathbf{k}) = \text{Re}[E_0](\mathbf{k})$ [$R_y(\mathbf{k}) = \text{Im}[E_0](\mathbf{k})$], where $E_0(\mathbf{k}) = 1 + e^{i\mathbf{k}\cdot\mathbf{b}_1} + e^{i\mathbf{k}\cdot\mathbf{b}_2}$ [$\mathbf{b}_1 = a(1/2, \sqrt{3}/2)$, $\mathbf{b}_2 = a(-1/2, \sqrt{3}/2)$]. For this investigation, the lattice constant was set as $a = 1$. By diagonalizing the Hamiltonian, the band dispersions can be obtained as

$$E_{0,\sigma}(\mathbf{k}) = \sqrt{R_x(\mathbf{k})^2 + R_y(\mathbf{k})^2 + R_{z,\sigma}(\mathbf{k})^2},$$

$$E_{1,\sigma}(\mathbf{k}) = -\sqrt{R_x(\mathbf{k})^2 + R_y(\mathbf{k})^2 + R_{z,\sigma}(\mathbf{k})^2}. \quad (33)$$

$$(34)$$

The zeros of the Green functions are given as

$$\zeta_{0,\sigma}(\mathbf{k}) = -R_{z,\sigma}(\mathbf{k}),$$

$$\zeta_{1,\sigma}(\mathbf{k}) = R_{z,\sigma}(\mathbf{k}). \quad (35)$$

In Fig. 3(b)-(d), the band dispersions and zeros of the diagonal components of the Green functions are plotted for the up spin ($E_{i,\uparrow}$, $\zeta_{i,\uparrow}$). In the Kane-Mele model, spin-orbit coupling λ_{SO} induces the \mathbb{Z}_2 topological insulators⁷, while the staggered charge potential Δ destroys the topological insulator. By changing Δ , the zeros of the Green function can be monitored in terms of how they behave in the topological and trivial insulator.

In Fig. 3(b), it is demonstrated that the zeros cross in the \mathbb{Z}_2 topological insulator as in the Chern insulator. Because the \mathbb{Z}_2 topological insulator in the Kane-Mele model without the Rashba term is the spin Chern insulator, the crosses of the zeros are guaranteed by the existence of the spin Chern number.

By increasing the strength of the staggered charge potential Δ , the insulator changes into the band insulator at $\Delta_c = 3\sqrt{3}\lambda_{\text{SO}}$. At the transition point, the crosses of the zeros are lifted at the Dirac point K' [Fig. 3(c)] and there is no cross in the trivial insulator [Fig. 3(d)]. By using the same argument that is shown in Sec. III C, it is demonstrated the cross of the zeros is gauge invariant.

B. Effects of Rashba term

This subsection considers the effects of the Rashba term. By adding the Rashba term, the Hamiltonian becomes 4×4 and the spin Chern number is no longer well defined. The Hamiltonian with the Rashba term is given as

$$H_R = \begin{pmatrix} R_{z,\uparrow}(\mathbf{k}) & R_\perp(\mathbf{k}) & 0 & z(\mathbf{k}), \\ R_\perp(\mathbf{k})^* - R_{z,\uparrow}(\mathbf{k}) & w(\mathbf{k}) & 0 & \\ 0 & w(\mathbf{k})^* & R_{z,\downarrow}(\mathbf{k}) & R_\perp(\mathbf{k}), \\ z(\mathbf{k})^* & 0 & R_\perp(\mathbf{k})^* - R_{z,\downarrow}(\mathbf{k}) & \end{pmatrix},$$

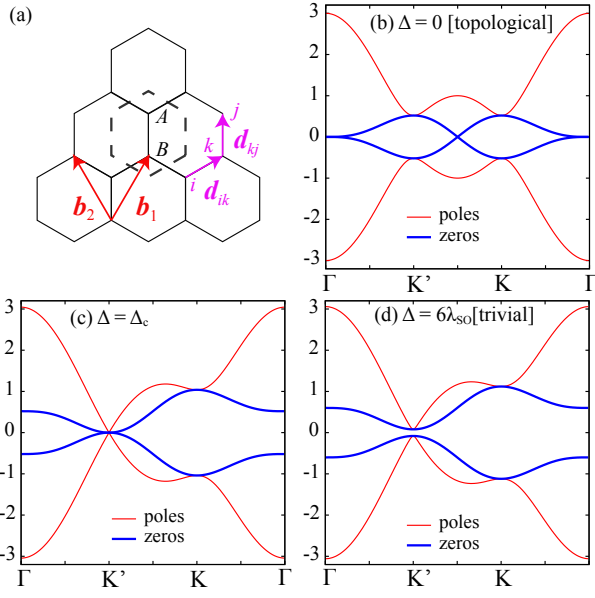


FIG. 3: (a) Lattice structure and translational vectors used in the Kane-Mele model. (b)–(d) Band dispersions and the zeros of the Green functions in the Kane-Mele model ($\lambda_{SO} = 0.1$). The red lines display the band dispersions. The thick blue lines represent the zeros of the Green function. For simplicity, only the zeros and poles for the up spin are shown.

where $R_{\perp}(\mathbf{k}) = R_x(\mathbf{k}) - iR_y(\mathbf{k})$, and

$$z(\mathbf{k}) = \lambda_R [(-i(1 - c_x c_y) + c_x s_y) / \sqrt{3} + s_x s_y + i s_x c_y],$$

$$w(\mathbf{k}) = \lambda_R [(i(1 - c_x c_y) + c_x s_y) / \sqrt{3} - s_x s_y + i s_x c_y].$$

Here, we defined $c_x [s_x]$ as $\cos(k_x/2)$ [$\sin(k_x/2)$] and $c_y [s_y]$ as $\cos(\sqrt{3}k_y/2)$ [$\sin(\sqrt{3}k_y/2)$]. For the Hamiltonian, because it is difficult to obtain the simple analytical form of the eigenvalues and the zeros, they were numerically obtained.

Even under the existence of the Rashba term, the crosses of zeros appear in the topological insulator as shown in Fig. 4(a) while the crosses disappear in the trivial insulators occur as shown in Fig. 4(b). At the K' point, the first and fourth zeros in the bandgap coincide with the valence bands, while the second and third zeros coincide with the conduction bands. At the K point, since the sign of the mass term is the opposite from the K' point, the opposite occurs. To connect each zero consistently, the first and the fourth zeros and the second and third zeros should traverse the bandgap and should cross at least once as shown in Fig. 4(a). These results indicate that the zeros of the Green function are also useful for characterizing the \mathbb{Z}_2 topological insulator.

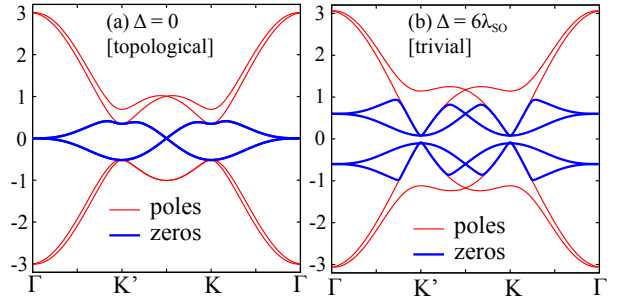


FIG. 4: Band dispersions and zeros of the Green functions in the Kane-Mele model with the Rashba term ($E_{SO} = 0.1$ and $E_R = 0.1$) for (a) the topological insulator and (b) the trivial insulator. The red lines display the band dispersions. The thick blue lines represent the zeros of the Green function. Only the zeros of Green functions in the bandgap are presented.

C. \mathbb{Z}_2 topological insulator in three dimensions (class AII)

This subsection considers the zeros of the Green functions in the three-dimensional topological insulators. A typical model of the three-dimensional topological insulator on the cubic lattice³⁴ is given as follows.

$$R_0 = M_0 + 3 - (\cos k_x + \cos k_y + \cos k_z), \quad (36)$$

$$R_1 = \sin k_x, \quad (37)$$

$$R_2 = \sin k_y, \quad (38)$$

$$R_3 = \sin k_z, \quad (39)$$

$$H = R_0 \alpha^0 + R_1 \alpha^1 + R_2 \alpha^2 + R_3 \alpha^3 \quad (40)$$

$$= \begin{pmatrix} R_0 & 0 & R_3 & R_1 - iR_2 \\ 0 & R_0 & R_1 + iR_2 & -R_3 \\ R_3 & R_1 - iR_2 & -R_0 & 0 \\ R_1 + iR_2 & -R_3 & 0 & -R_0 \end{pmatrix} \quad (41)$$

In this model, the \mathbb{Z}_2 topological insulator is achieved for $-2 < M_0 < 0$ and $-6 < M_0 < -4$ while the trivial insulator is realized for $M_0 < -6$ and $M_0 > 0$. The weak \mathbb{Z}_2 topological insulator is obtained for $-4 < M_0 < -2$.

The eigenvalues are given as follows.

$$E_0 = \sqrt{R_0^2 + R_1^2 + R_2^2 + R_3^2}, \quad (42)$$

$$E_1 = -\sqrt{R_0^2 + R_1^2 + R_2^2 + R_3^2} \quad (43)$$

It can be noted that the eigenvalues are doubly degenerate. The zeros of the Green function in the bandgap are given as follows.

$$\zeta_0 = -R_0, \quad (44)$$

$$\zeta_1 = R_0.$$

From these expressions, it can be shown that the zeros and the poles coincide at eight time reversal points, such

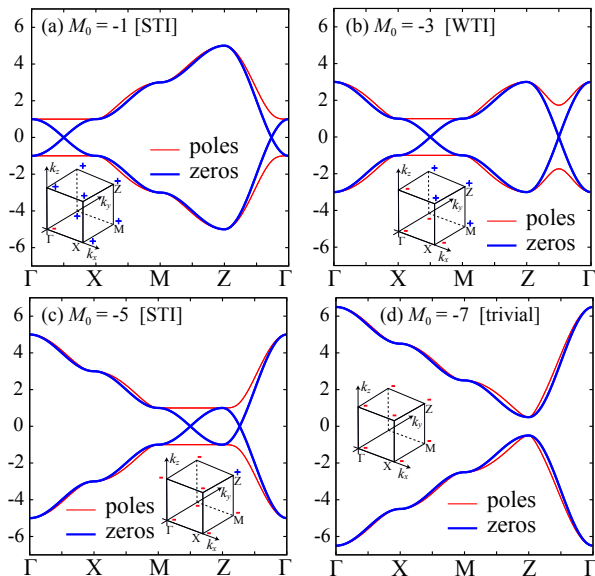


FIG. 5: Band dispersions and zeros of the Green functions in the Hamiltonian defined in Eq. (41) for (a) a strong topological insulator, (b) a weak topological insulator, (c) a strong topological insulator, (d) and a trivial insulator. The red lines display the band dispersions, and the thick blue lines represent the zeros of the Green function. In the inset, $\eta(\mathbf{k})$ is shown for the time-reversal points. STI (WTI) is an abbreviation for a strong (weak) topological insulator.

as the Γ , X, and Z points. To analyze the crosses of the zeros, the following was defined.

$$\eta(\mathbf{k}) = \text{sign}(\zeta_1(\mathbf{k})). \quad (45)$$

If $\eta(\mathbf{k}) = 1$ ($\eta(\mathbf{k}) = -1$) at the time reversal point, $\zeta_1(\mathbf{k})$ coincides with $E_0(\mathbf{k})$ ($E_1(\mathbf{k})$). $\eta(\mathbf{k})$ at the time reversal points are shown in the inset.

Because $\zeta_0(\mathbf{k}) = -\zeta_1(\mathbf{k})$, they cross between $\eta(\mathbf{k}) = 1$ and $\eta(\mathbf{k}) = -1$. For example, for $M_0 = -1$ [Fig. 5(a)], they cross between Γ point and X point. Even for the weak topological region, they cross as shown in Fig. 5(a) and they do not cross in the trivial insulators. These results indicate that the crosses of the zeros can be useful for detecting the topological phases for strong and weak topological insulators since the crosses are guaranteed by the existence of the gapless surface states.

D. Intuitive argument for explaining the cross of the zeros

In this section, we provide an intuitive discussion on the zeros of the Green functions. We can consider the three-dimensional Dirac electrons, for which the effective

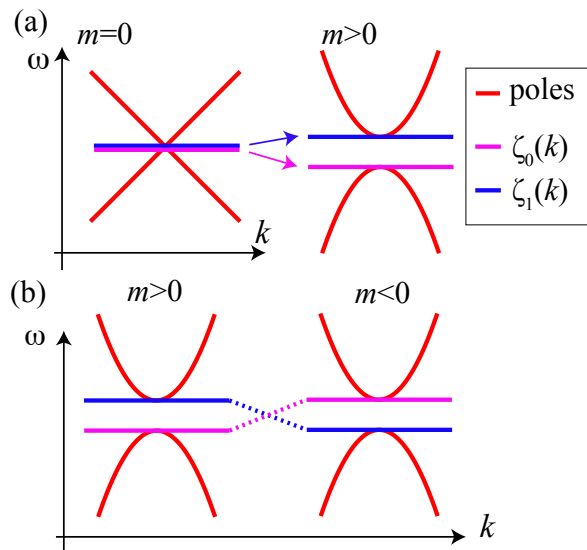


FIG. 6: (a) Schematic picture of the band dispersions and zeros around the massless ($m = 0$) and massive ($m > 0$) Dirac electrons. (b) Schematic of the band dispersions and zeros at different momenta.

Hamiltonian around the Dirac point is defined as

$$H_D = m\alpha_0 + \sum_{i=1,2,3} k_i \alpha^i, \quad (46)$$

$$\alpha_0 = \begin{pmatrix} I & 0 \\ 0 & -I \end{pmatrix}, \quad \alpha_1 = \begin{pmatrix} 0 & \sigma_x \\ \sigma_x & 0 \end{pmatrix}, \quad (47)$$

$$\alpha_2 = \begin{pmatrix} 0 & \sigma_y \\ \sigma_y & 0 \end{pmatrix}, \quad \alpha_3 = \begin{pmatrix} 0 & \sigma_z \\ \sigma_z & 0 \end{pmatrix}, \quad (48)$$

where k_i represents the momentum and m is the mass of the Dirac electrons. It is noted that the low-energy effective Hamiltonian can be reduced to the Dirac Hamiltonian by performing the proper unitary transformation. The doubly degenerate eigenvalues are given as

$$E_{\pm}(\mathbf{k}) = \pm(|\mathbf{k}|^2 + m^2)^{1/2}. \quad (49)$$

The zeros of the Green functions between E_+ and E_- are given as

$$\begin{aligned} \zeta_0(\mathbf{k}) &= -m, \\ \zeta_1(\mathbf{k}) &= m. \end{aligned} \quad (50)$$

The band dispersions and zeros around the Dirac points are shown in Fig. 6(a). From this behavior, it can be confirmed that the zeros and poles should coincide at the massless Dirac point ($\mathbf{k} = 0$), which is guaranteed by the Cauchy interlacing inequalities.

When the signs of the mass terms at different Dirac points are opposite, the zeros should traverse the bandgap and cross with another zero at least once in the bandgap (see Fig. 6(b)). This consideration offers

an intuitive interpretation of the crossing of the zeros in bulk systems of topological insulators, irrespective of the details of the systems. As we have already shown, the crosses of the zeros occur in the Chern insulator (class A) and the two- and three-dimensional \mathbb{Z}_2 topological insulators (class AII) in Sec. IV. The crosses also occur in the four-dimensional $2\mathbb{Z}$ topological insulators (class AI) as shown in Appendix C.

V. TOPOLOGICAL INSULATORS WITH CHIRAL SYMMETRY (CLASS AIII, BDI, CII)

Thus far, we examined the zeros of the Green functions in the topological insulators *without* chiral symmetry. Here, we examine the behavior of the zeros of the Green functions in the topological insulators *with* chiral symmetry.

For the Hamiltonian that has chiral symmetry, the unitary matrix Γ that anti-commutes with the Hamiltonian always exists, i.e.,

$$H\Gamma + \Gamma H = 0. \quad (51)$$

From this, the Hamiltonian with chiral symmetry and its Green function at zero energy can be described as a block off-diagonal form as demonstrated below.

$$H = \begin{pmatrix} 0 & Q \\ Q^\dagger & 0 \end{pmatrix}, \quad (52)$$

$$G(\omega = 0) = -H^{-1} = \begin{pmatrix} 0 & -(Q^\dagger)^{-1} \\ -Q^{-1} & 0 \end{pmatrix}. \quad (53)$$

In this representation, the unitary matrix Γ has a diagonal form, which is given as

$$\Gamma = \begin{pmatrix} I & 0 \\ 0 & -I \end{pmatrix}. \quad (54)$$

From Eq. (53), it can be observed that the zeros of the bulk Green function in the bandgap always exist at $\omega = 0$ for the topological and trivial insulators. This result indicates that it is impossible to distinguish the topological phase from the trivial phases if we take the block off-diagonal form of the Hamiltonians.

It can be observed that the ZEC still holds for the topological insulators with chiral symmetry because the zeros of the Green functions cross in all the momentum space in the chiral topological insulators. However, the zeros of the Green functions always exist $\omega = 0$ even for the trivial insulators, which seem to have no relation with the gapless edge states. To distinguish the topologically phases from the trivial phases in the chiral symmetric cases, it is necessary to employ the gauges that make the Hamiltonians *not* block off-diagonal form.

A simple way to obtain such a Hamiltonian is to perform the following unitary transformation to the block off-diagonal Hamiltonian

$$U = \frac{1}{\sqrt{2}} \begin{pmatrix} I & -I \\ I & I \end{pmatrix} \quad (55)$$

and the transformed Hamiltonian is given as follows.

$$\tilde{H} = U^\dagger H U = \frac{1}{2} \begin{pmatrix} Q + Q^\dagger & (Q - Q^\dagger) \\ -(Q - Q^\dagger) & -(Q + Q^\dagger) \end{pmatrix}. \quad (56)$$

From this transformation, the Hamiltonians have diagonal elements. Thus, the zeros are not constant in general and they can be useful for clarifying the topological phases as demonstrated below. It can be noted that the unitary matrix Γ has a block off-diagonal form in this gauge, i.e.,

$$\tilde{\Gamma} = U^\dagger \Gamma U = \begin{pmatrix} 0 & -I \\ -I & 0 \end{pmatrix}. \quad (57)$$

A. BDI and AIII topological insulators in one-dimension

As an example of the BDI and AIII topological insulators, the one-dimensional Hamiltonian^{35,36} can be considered, which is given as

$$H = \begin{pmatrix} 0 & R_x - iR_y \\ R_x + iR_y & 0 \end{pmatrix}, \quad (58)$$

where $R_x = 1 + \gamma \cos(x - \delta)$ and $R_y = \gamma \sin(x - \delta)$. When $\gamma > 1$ and $\delta = 0$, this system becomes a topological insulator ($d = 1$, BDI). If $\delta \neq 0$ and $\gamma > 1$, the system becomes an AIII topological insulator³⁶.

The eigenvalues of the Hamiltonian are given as follows.

$$E_0 = \sqrt{R_x^2 + R_y^2} \quad (59)$$

$$E_1 = -\sqrt{R_x^2 + R_y^2}. \quad (60)$$

Following the discussion above, the unitary transformation can be performed as follows.

$$\tilde{H} = U^\dagger H U = \begin{pmatrix} R_x & iR_y \\ -iR_y & -R_x \end{pmatrix}. \quad (61)$$

The zeros of the Green function for the transformed Hamiltonian \tilde{H} are given as follows.

$$\begin{aligned} \zeta_0 &= -R_x, \\ \zeta_1 &= R_x. \end{aligned} \quad (62)$$

For the BDI topological insulator ($\delta = 0, \gamma > 1$), the zeros cross in the bandgap as shown in Fig. 7(a) whereas the zeros do not cross in the trivial insulator. It can be confirmed that the same behavior occurs in the AIII topological insulators as shown in Fig. 7(c).

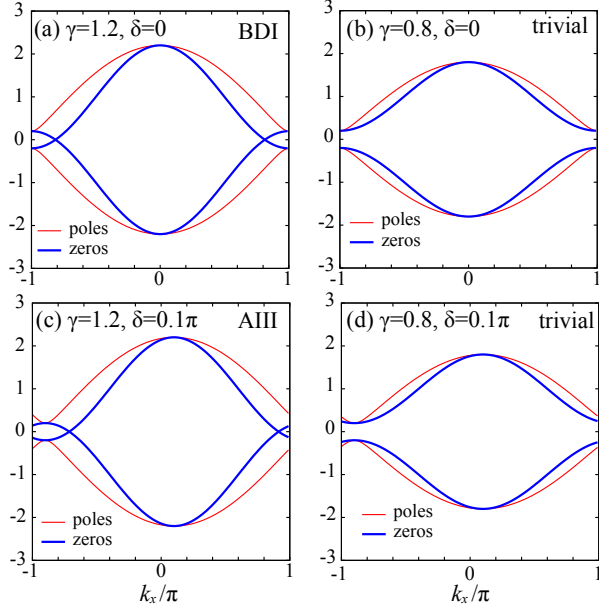


FIG. 7: Band dispersions and zeros of the Green functions in the model Hamiltonian for (a),(b) BDI, and (c),(d) AII topological insulators, which is defined in Eq. (58). The red lines display the band dispersions, and the thick blue lines represent the zeros of the Green function. The zeros cross in the bandgap for the BDI and AII topological insulators.

B. CII topological insulator in one-dimension

As an example of the CII topological insulators, the following four-orbital models were applied³⁷.

$$H = \begin{pmatrix} 0 & 0 & R_x & iA + R_y \\ 0 & 0 & iA + R_y & R_x \\ R_x & -iA + R_y & 0 & 0 \\ -iA + R_y & R_x & 0 & 0 \end{pmatrix}, \quad (63)$$

where $R_x = t_\perp$, $R_y = 2t \sin k_x$, and $A = s + 2s' \cos k_x$. When $(t_\perp/t)^2 + (s/s')^2 < 4$, this system becomes a topological insulator ($d = 1$, CII). The eigenvalues of the Hamiltonian are given as follows.

$$E_0 = -\sqrt{(R_x + R_y)^2 + A^2}, \quad (64)$$

$$E_1 = -\sqrt{(R_x - R_y)^2 + A^2}, \quad (65)$$

$$E_2 = \sqrt{(R_x - R_y)^2 + A^2}, \quad (66)$$

$$E_3 = \sqrt{(R_x + R_y)^2 + A^2}. \quad (67)$$

Following the discussion above, we take the gauge that

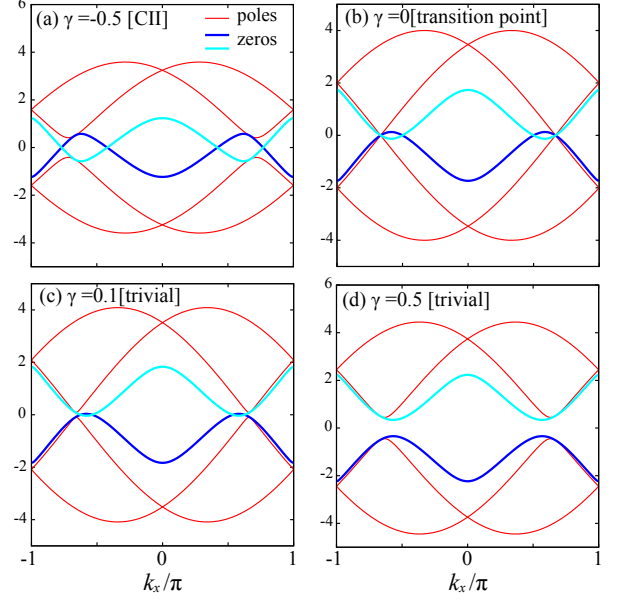


FIG. 8: Band dispersions and zeros of the Green functions in the model defined in Eq. (68) for the (a) topological insulator, (b) transition point, (c) trivial insulator, (d) and the trivial insulator. For this investigation, $t = 1$, $s = s' = 1$, and $t_\perp = \sqrt{4 - (s/s')^2} + \gamma$. For $\gamma < 0$ ($\gamma > 0$), the system becomes a topological (trivial) insulator. The red lines display the band dispersions, and the thick blue lines represent the zeros of the Green function.

makes Γ block the off-diagonal form.

$$\tilde{H} = U^\dagger H U = \begin{pmatrix} R_x & R_y & 0 & iA \\ R_y & R_x & iA & 0 \\ 0 & -iA & -R_x & -R_y \\ -iA & 0 & -R_y & -R_x \end{pmatrix} \quad (68)$$

The zeros of the Green function of \tilde{H} are not given in a simple analytical form. Thus, the zeros can be numerically obtained, and they are shown in Fig. 8.

As illustrated in Fig. 8(a), in the CII topological insulator, the zeros of the Green functions cross in the bandgap. Basically, the crosses vanish in the trivial insulator sufficiently away from the transition point. However, the accidental crosses of the zeros still survive, even in the trivial insulators as shown in Fig. 8(c) near the transition point. This result indicates that the crosses of the zeros do not necessarily indicate the gapless edge states.

VI. HIGHER-ORDER TOPOLOGICAL INSULATORS

As demonstrated in the previous sections, the zeros cross in the topological insulators because the gapless edge states inevitably induce the crossing of the zeros. Recently, new classes of the topological insulators have

been found, such as the higher-order topological insulators^{25,26}. In the higher-order topological insulators in n dimensions, the gapless edge states appear below $n - 2$ dimensions. For example, the three-dimensional higher-order topological insulators have one-dimensional edge states and the two-dimensional higher-order topological insulators have zero-dimensional edge states. In this section, we demonstrate that the crosses of the zeros in the bulk system also appear in the higher-order topological insulators because they have gapless edge states.

A. Higher-order topological insulators in three dimensions

A model of the three-dimensional higher-order topological insulator on the cubic lattice is described as follows²⁶.

$$R_0 = M + (\cos k_x + \cos k_y + \cos k_z), \quad (69)$$

$$R_1 = \sin k_x, \quad (70)$$

$$R_2 = \sin k_y, \quad (71)$$

$$R_3 = \sin k_z, \quad (72)$$

$$R_4 = \Delta_2(\cos k_x - \cos k_y), \quad (73)$$

$$H = R_0\alpha^0 + R_1\alpha^1 + R_2\alpha^2 + R_3\alpha^3 + R_4\tau_y\sigma_0 \quad (74)$$

$$= \begin{pmatrix} R_0 & 0 & R_3 - iR_4 & R_1 - iR_2 \\ 0 & R_0 & R_1 + iR_2 & -R_3 - iR_4 \\ R_3 + iR_4 & R_1 - iR_2 & -R_0 & 0 \\ R_1 + iR_2 & -R_3 + iR_4 & 0 & -R_0 \end{pmatrix} \quad (75)$$

The eigenvalues are given as

$$E_0 = \sqrt{R_0^2 + R_1^2 + R_2^2 + R_3^2 + R_4^2}, \quad (76)$$

$$E_1 = -\sqrt{R_0^2 + R_1^2 + R_2^2 + R_3^2 + R_4^2}, \quad (77)$$

and the zeros are given as

$$\zeta_0 = -R_0, \quad (78)$$

$$\zeta_1 = R_0. \quad (79)$$

It can be noted that without R_4 , this model is the same as that of the three-dimensional \mathbb{Z}_2 topological insulators defined in Eq. (41). It is shown that the system changes from the \mathbb{Z}_2 topological insulator into a higher-order topological insulator when R_4 is added²⁶.

As shown in Fig. 9, the crosses of the zeros exist even for the higher-order topological insulators. Although R_4 lifts the coincidences of the zeros and poles at some k points such as X, the coincidences still exist for Γ , M, and Z.

B. Higher-order topological insulators in two dimensions

As an example of the two-dimensional higher-order topological insulators²⁵, we consider the following Hamil-

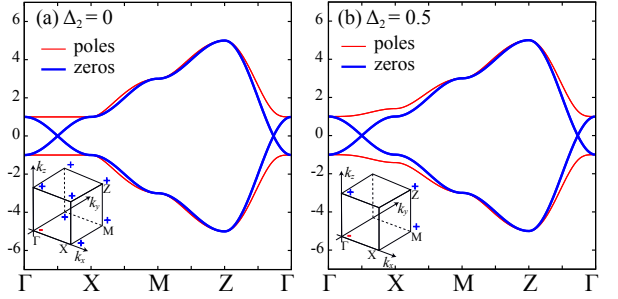


FIG. 9: Band dispersions (thin red curves) and zeros (thick blue curves) of the Green functions in the model Hamiltonians for the three-dimensional higher-order topological insulators defined in Eq. (75). For (a) $\Delta_2 = 0$, the system is a \mathbb{Z}_2 topological insulator and the system becomes HOTI for (b) $\Delta_2 = 0.5$.

tonian.

$$H = \begin{pmatrix} 0 & 0 & iR_z + A & iR_x + R_y \\ 0 & 0 & iR_x - R_y - iR_z + A & 0 \\ -iR_z + A - iR_x - R_y & 0 & 0 & 0 \\ -iR_x + R_y & iR_z + A & 0 & 0 \end{pmatrix} \quad (80)$$

where $R_x = E \sin k_y$, $R_y = \gamma + E \cos k_y$, $R_z = E \sin k_x$, and $A = \gamma + E \cos k_x$. The eigenvalues are given as

$$E_0 = \sqrt{A^2 + R_x^2 + R_y^2 + R_z^2}, \quad (81)$$

$$E_1 = -\sqrt{A^2 + R_x^2 + R_y^2 + R_z^2}. \quad (82)$$

Because the system has chiral symmetry, according to a similar manner for the 1D chiral topological insulators, the unitary transformation can be performed using

$$U = \frac{1}{\sqrt{2}} \begin{pmatrix} I & -I \\ I & I \end{pmatrix}. \quad (83)$$

and obtain

$$\tilde{H} = U^\dagger H U = \begin{pmatrix} A & 0 & iR_z & iR_x + R_y \\ 0 & A & iR_x - R_y & -iR_z \\ -iR_z & -iR_x - R_y & -A & 0 \\ -iR_x + R_y & iR_z & 0 & -A \end{pmatrix}. \quad (84)$$

In this modified Hamiltonian, the zeros in the bandgap are given as

$$\zeta_0 = -A, \quad (85)$$

$$\zeta_1 = A. \quad (86)$$

As shown in Fig. 10, the zeros cross in the higher-order topological insulator while they do not cross in the trivial insulator. This result indicates that the cross of the zeros in the bulk system is useful for detecting the higher-order topological phases.

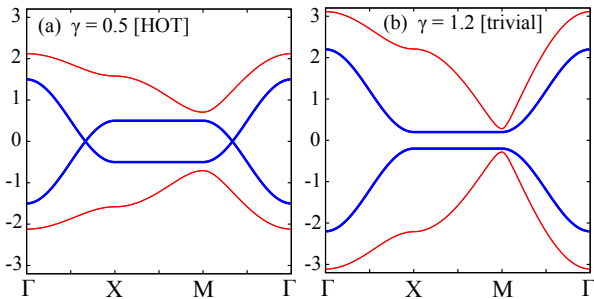


FIG. 10: Band dispersions (thin red curves) and zeros (thick blue curves) of the Green functions in the model for two-dimensional higher-order topological insulators for (a) $\Gamma = 0.5$ and (b) $\Gamma = 1.2$.

C. Higher-order topological insulator in the Fu-Kane-Mele model under a magnetic field

Finally, we examine how the zeros of the Green functions behave in the Fu-Kane-Mele model under a magnetic field³⁸⁻⁴⁰, which is defined as follows.

$$R_1 = 1 + \delta t_1 + [\cos k_1 + \cos k_2 + \cos k_3], \quad (87)$$

$$R_2 = \sin k_1 + \sin k_2 + \sin k_3, \quad (88)$$

$$R_3 = \lambda_{\text{SO}}[\sin k_2 - \sin k_3 - \sin(k_2 - k_1) + \sin(k_3 - k_1)], \quad (89)$$

$$R_4 = \lambda_{\text{SO}}[\sin k_3 - \sin k_1 - \sin(k_3 - k_2) + \sin(k_1 - k_2)], \quad (90)$$

$$R_5 = \lambda_{\text{SO}}[\sin k_1 - \sin k_2 - \sin(k_1 - k_3) + \sin(k_2 - k_3)], \quad (91)$$

$$H = \begin{pmatrix} R_5 + h_z & R_1 - iR_2 & R_3 - iR_4 & 0 \\ R_1 + iR_2 & -R_5 + h_z & 0 & -R_3 + iR_4 \\ R_3 + iR_4 & 0 & -R_5 - h_z & R_1 - iR_2 \\ 0 & R_3 - iR_4 & R_1 + iR_2 & R_5 - h_z \end{pmatrix}, \quad (92)$$

where $k_1 = k_y + k_z$, $k_2 = k_x + k_z$, $k_3 = k_x + k_y$, and h_z represent the magnetic field.

It is shown that the three-dimensional \mathbb{Z}_2 topological insulator appears in the Fu-Kane-Mele model. The gapless surface states are gapped out when the magnetic field is applied because the magnetic field breaks the time-reversal symmetry. Nevertheless, by analyzing the entanglement spectrum, Turner *et al.* showed that the topological properties of the systems still remain⁴⁰. They demonstrated that the entanglement spectrum behaves as gapless surface states, even under a magnetic field. Recently, it has been established that the one-dimensional hinge states appear in the \mathbb{Z}_2 topological insulator under a magnetic field^{41,42}. The higher-order topological nature is the origin of the characteristic behavior in the entanglement spectrum. Here, we show that the zeros of the Green functions can also capture the higher-order topological insulator in this system.

In Fig. 11(a) and (b), the bulk band dispersions and the zeros of the Green functions for $h_z = 0$ and $h_z = 0.2$, respectively, are presented. For this investigation, $\delta t = 0.5$ and $\lambda_{\text{SO}} = 0.25$. Even under the finite magnetic field, it was determined that the crosses of the zeros of the Green functions can still survive. According to the ZEC, the crosses indicate that the existence of the gapless surface/edge states.

To observe this, the two-dimensional surface states and the one-dimensional hinge states were calculated in Fig. 11(c)-(f). As shown in Fig. 11(d), the gapless surface states are gapped out by the magnetic field. However, as shown in Fig. 11(f), the gapless one-dimensional edge (hinge) states appear under the magnetic field. This result shows that a higher-order topological insulator is realized in the Fu-Kane-Mele model under the magnetic field and is captured by the crosses of the zeros.

VII. SUMMARY

In summary, this study focused on the zeros of the diagonal components of the Green functions in topological insulators. Based on the arguments that were used in the eigenvector-eigenvalue identity²³, it was first demonstrated that the zeros of the diagonal components of the Green functions are given by the eigenvalues of the minor matrix M_n , which is obtained by removing the n th row and column from the original Hamiltonian. This mathematical foundation offers an efficient way to study the zeros of the Green functions both analytically and numerically.

For a two-dimensional Chern insulator, which is a canonical model of two-dimensional a topological insulator, it is established that the cross of the zeros is a key to distinguishing topological insulators from trivial insulators. For the Chern insulators, this study has explicitly shown that the existence of the Chern number guarantees the cross of the zeros in bulk systems. It has been demonstrated that the cross of the zeros is gauge invariant, although the positions of the zeros are not. We have also shown that the cross of the zeros in the bulk system is induced by the gapless edge states (zero-edge correspondence [ZEC]). This relation can be regarded as another description of the bulk-edge correspondence²⁴, and it can be useful to detect gapless edge states. It was observed that the crosses of the zeros can occur in the other class of the topological insulators without chiral symmetries such as the \mathbb{Z}_2 (class AII) topological insulators in two and three dimensions and $2\mathbb{Z}$ (class AI) topological insulators in four dimensions. The intuitive argument for explaining the cross of the zeros in the topological insulators is also demonstrated.

For topological insulators with chiral symmetry, this study demonstrated that the zeros also cross in the bandgap when we take suitable gauges that make the Hamiltonians not block off-diagonal form (in other words, the chiral matrix Γ has an off-diagonal form). By tak-

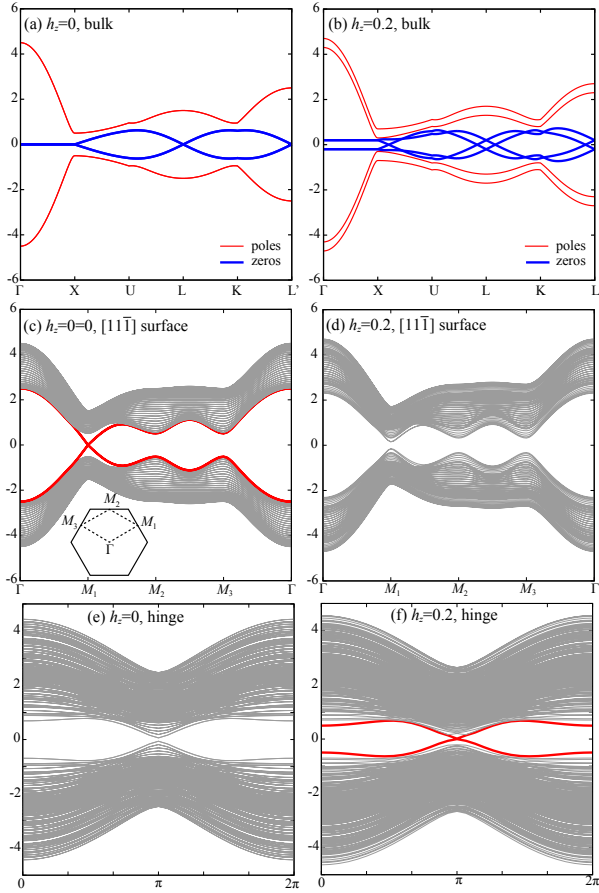


FIG. 11: Band dispersions (thin red curves) and zeros (thick blue curves) of the Green functions in the Fu-Kane-Mele model for (a) $h_z = 0$ and (b) $h_z = 0.2$. For this study, $\delta t = 0.5$ and $\lambda_{\text{SO}} = 0.25$. The crosses of the zeros survive even under finite magnetic fields. Band dispersions in the slab geometry ($[11\bar{1}]$ surface) in the Fu-Kane-Mele model for (c) $h_z = 0$ and (d) $h_z = 0.2$. Surface states (thick red curves shown in (c)) are gapped out by the magnetic field. Band dispersions in the hinge geometry in the Fu-Kane-Mele model for (e) $h_z = 0$ and (f) $h_z = 0.2$. Gapless hinge states appear for $h_z = 0.2$, which is consistent with the ZEC. The unit vectors were employed as $\mathbf{a}_1 = (0, 1, 1)$, $\mathbf{a}_2 = (1, 0, 1)$, and $\mathbf{a}_3 = (1, 1, 0)$. To realize the $[11\bar{1}]$ surface (the one-dimensional hinge state), the periodicity was cut for \mathbf{a}_3 (\mathbf{a}_2 and \mathbf{a}_3). The calculations of the surface and hinge states were performed using PythTB⁴³.

ing the model Hamiltonians for class BDI, AIII, and CII topological insulators, this investigation has shown that the crosses of the zeros always occur in topological phases. These are consistent with the fact that the gapless edge states induce the crosses of the zeros in the bulk Green functions.

Since the crosses of the zeros are guaranteed by the existence of the gapless edge state, it is expected that this is useful for detecting other exotic topological phases, which are not listed in the conventional periodic table for

topological insulators (Table I). As an example of these exotic topological phases, we consider the higher-order topological insulators. The cross of the zeros is also useful for detecting the higher-order topological insulators in two and three dimensions.

The comprehensive analysis in this study demonstrates that the zeros of the Green functions can be used as a simple visual detection tool for topological phases. It may be useful when searching for new topological phases because the crosses of the zeros can be easily detected without any assumptions. In addition, since this method does not require full gap states but only needs the cross of the zeros, the zeros of the Green functions can be useful to identify the exotic gapless edge states that appear in topological semimetals such as the Weyl^{44–47} and the Topological Dirac semimetals^{48–50}.

It needs to be noted that the accidental crosses of the zeros in the trivial phases may occur, as demonstrated for the CII topological insulator. We emphasize that this is *not* in conflict with the ZEC. In the ZEC, the gapless edge states induce the cross of the zeros in the bulk Green functions. The converse of the ZEC does not hold. Nevertheless, the cross of the zeros of the bulk Green function is still useful when searching for the topological phases since the absence of the crosses indicates that the system is not topological in the sense that they have no gapless edge states. This fact may be useful in the screening process for searching the topological materials by combining with the high-through *ab initio* calculations^{18–20,22}.

This study was restricted to the analysis of topological insulators for simplicity; however, a similar analysis is possible for topological superconductors. Furthermore, a similar analysis might be possible for the disordered^{51,52} and interacting^{27,53,54} systems because the Green functions for the correlated and/or disordered systems are well-defined. These unexplored issues are intriguing but need to be further investigated.

Acknowledgments

This work was supported by JSPS KAKENHI. (Grant Nos. JP16H06345, JP19K03739, and JP20H01850). T.M. thanks Masafumi Udagwa, Yutaka Akagi, and Satoru Hayami for fruitful discussions in the early stage of this study. T.M. would also like to thank Yi Zhang for the valuable discussion on Ref. [40]. T.M. was also supported by the Building of Consortia for the Development of Human Resources in Science and Technology from the MEXT of Japan.

Appendix A: Proof of the Cauchy interlacing inequalities

Although the proof of the Cauchy interlacing inequalities is shown in the literature^{30,31}, we have provided another proof of the inequalities based on the structure of

the Green functions to make this paper self-contained. To prove the Cauchy interlacing inequalities, the definition the Green function (Eq. (2)) is rewritten as

$$G_n(\mathbf{k}, \omega) = \frac{N_n(\mathbf{k}, \omega)}{\prod_i (\omega - E_i)}, \quad (\text{A1})$$

$$N_n(\mathbf{k}, \omega) = \sum_j |\Psi_j^{(n)}|^2 \prod_{i \neq j} (\omega - E_i). \quad (\text{A2})$$

The roots of the $(n-1)$ th polynomial $N_n(\mathbf{k}, \omega)$ correspond to the zeros of $G_n(\mathbf{k}, \omega)$, i.e., the eigenvalues of the minor matrix $M_n(\mathbf{k})$.

From Eq. (A2), it can be shown that $N_n(\mathbf{k}, \omega)$ changes its sign between $E_i(\mathbf{k})$ and $E_{i+1}(\mathbf{k})$, i.e., $N_n(\mathbf{k}, E_i(\mathbf{k})) \cdot N_n(\mathbf{k}, E_{i+1}(\mathbf{k})) < 0$ unless $|\Psi_i^{(n)}| = 0$ or $|\Psi_{i+1}^{(n)}| = 0$. This indicates that the $N_n(\mathbf{k}, \omega)$ has at least one real root between $E_i(\mathbf{k})$ and $E_{i+1}(\mathbf{k})$. Because the $N_n(\mathbf{k}, \omega)$ is the $(n-1)$ th polynomial with respect to ω , the number of roots should be one. For $|\Psi_i^{(n)}(\mathbf{k})| = 0$, $\omega = E_i(\mathbf{k})$ is a root of $N_n(\mathbf{k}, \omega)$. This is consistent with the eigenvalue-eigenvector identity.

Thus, for both $|\Psi_n^i| = 0$ and $|\Psi_n^i| \neq 0$, $N_n(\mathbf{k}, \omega)$ has one real root between $E_i(\mathbf{k})$ and $E_{i+1}(\mathbf{k})$. In other words, one zero of $G_n(\mathbf{k}, \omega)$ should exist between every adjacent eigenvalue (poles of the Green function). This was also pointed out in a previous study⁴. This represents the Cauchy interlacing inequalities.

Appendix B: Proof of the zero-edge correspondence m -orbital system

The bulk Hamiltonian for the m -orbital system is given as

$$H_{\text{bulk}} = \begin{pmatrix} A & B \\ B^\dagger & H_{\text{edge}} \end{pmatrix}, \quad (\text{B1})$$

where the size of A is $m \times m$, the size of B is $n \times m$, and the size of H_{edge} is $n \times n$. As we explained in Sec. III D, H_{edge} describes the system with the edges or surfaces. It is assumed that n is sufficiently larger than m . By using the unitary matrix that diagonalizes H_{edge} , the Hamiltonian can be transformed as

$$\tilde{H}_{\text{bulk}} = \begin{pmatrix} I & 0 \\ 0 & U^\dagger \end{pmatrix} \begin{pmatrix} A & B \\ B^\dagger & H_{\text{edge}} \end{pmatrix} \begin{pmatrix} I & 0 \\ 0 & U \end{pmatrix} \quad (\text{B2})$$

$$= \begin{pmatrix} A & \tilde{B} \\ \tilde{B}^\dagger & D \end{pmatrix} \quad (\text{B3})$$

$$D = \text{diag}(E_0, E_1, \dots, E_{n-1}), \quad (\text{B4})$$

where E_i represents the i th eigenvalue of H_{edge} .

Here, it is assumed that H_{edge} has m degenerate eigenvalues. Without loss of generality, it can be assumed that $E = E_0 = E_1 = \dots = E_{m-1}$. The following form of the

inverse of the bulk Green function can be obtained.

$$\tilde{G}_{\text{bulk}}(\omega = E)^{-1} = (EI - \tilde{H}) = \begin{pmatrix} G_A(E)^{-1} & \tilde{F} & \tilde{C} \\ \tilde{F}^\dagger & 0_{m \times m} & 0 \\ \tilde{C}^\dagger & 0 & \tilde{G}_{D_{n-m}}(E)^{-1} \end{pmatrix}, \quad (\text{B5})$$

where $G_A(E)^{-1} = (EI - A)$, $\tilde{G}_{D_{n-m}}(E)^{-1} = (EI - D_{n-m})$, and $D_{n-m} = \text{diag}(E_m, \dots, E_{n-1})$. From this, the bulk Green function can be expressed as

$$\tilde{G}_{\text{bulk}}(\omega = E) = \begin{pmatrix} 0_{m \times m} & (\tilde{F}^\dagger)^{-1} & 0 \\ \tilde{F}^{-1} & X & -\tilde{F}^{-1} \tilde{C} \tilde{G}_{D_{n-m}} \\ 0 & -\tilde{G}_{D_{n-m}} \tilde{C}^\dagger (\tilde{F}^\dagger)^{-1} & \tilde{G}_{D_{n-m}} \end{pmatrix}, \quad (\text{B6})$$

$$X = -\tilde{F}^{-1} G_A^{-1} (\tilde{F}^\dagger)^{-1} + \tilde{F}^{-1} \tilde{C} \tilde{G}_{D_{n-m}} \tilde{C}^\dagger (\tilde{F}^\dagger)^{-1}, \quad (\text{B7})$$

where we assume that \tilde{F}^{-1} exists.

$\tilde{G}_{\text{bulk}}(\omega = E)$ can be rewritten as

$$\tilde{G}_{\text{bulk}}(\omega = E) = \begin{pmatrix} 0_{m \times m} & b \\ b^\dagger & \tilde{X} \end{pmatrix}. \quad (\text{B8})$$

By using the relation

$$G_{\text{bulk}}(E) = (EI - H_{\text{bulk}})^{-1} = \tilde{U} \tilde{G}_{\text{bulk}} \tilde{U}^\dagger, \quad (\text{B9})$$

$$\tilde{U} = \begin{pmatrix} I & 0 \\ 0 & U \end{pmatrix}, \quad (\text{B10})$$

we can obtain

$$G_{\text{bulk}} = \begin{pmatrix} 0_{m \times m} & bU^\dagger \\ Ub^\dagger & U\tilde{X}U^\dagger \end{pmatrix}. \quad (\text{B11})$$

Therefore, the zeros of the bulk Green function have m degeneracies if H_{edge} has m degenerate eigenvalues.

Appendix C: AI topological insulator in four dimensions

According to the periodic table for the topological insulators, the AI topological insulator does not appear in the realistic dimensions ($d = 1, 2, 3$), but it appears in four dimensions. The model Hamiltonian is proposed in Ref. [55]. Its realization in the electric circuits has been proposed⁵⁶. The Hamiltonian for the AI topological insulators is given as

$$H = \begin{pmatrix} M & 0 & R_z - iA & R_x - iR_y \\ 0 & M & R_x + iR_y & -R_z - iA \\ R_z + iA & R_x - iR_y & -M & 0 \\ R_x + iR_y & -R_z + iA & 0 & -M \end{pmatrix}, \quad (\text{C1})$$

where $R_x = 2 \cos k_z + \cos k_w$, $R_y = \sin k_w$, $R_z = 2 \cos k_x + \cos k_y$, $A = \sin k_y$, and $M = m +$

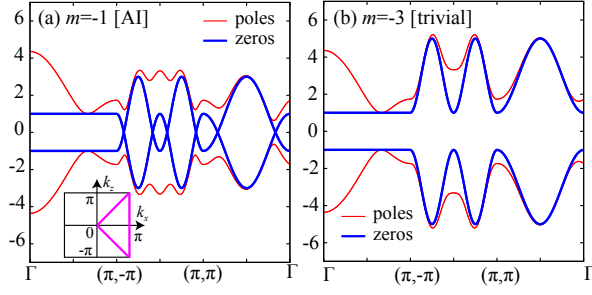


FIG. 12: Band dispersions and zeros of the Green functions in the model defined in Eq. (C1) for the (a) topological phase and (b) the trivial phase. For this study, $J' = 1$, $J'' = 0$, and $k_y = k_w = 0$. For $-2J' < m < J'$ ($J'' = 0$), the system becomes a topological insulator. In the inset, the symmetry line that was used in the plot is illustrated. The zeros cross in the bandgap in the AI topological insulators.

$2J' \cos(2k_x + 2k_z) + 2J'' \cos(2k_x - 2k_z)$. It can be noted that k_w is the momentum in the fourth dimension.

The eigenvalues (doubly degenerate) are given by

$$E_0 = \sqrt{M^2 + A^2 + R_x^2 + R_y^2 + R_z^2}, \quad (C2)$$

$$E_1 = -\sqrt{M^2 + A^2 + R_x^2 + R_y^2 + R_z^2}, \quad (C3)$$

and the zeros of the Green functions are given by

$$\begin{aligned} \zeta_0 &= -M \\ &= -(m + 2J' \cos(2k_x + 2k_z) + 2J'' \cos(2k_x - 2k_z)), \quad (C4) \\ \zeta_1 &= M \\ &= m + 2J' \cos(2k_x + 2k_z) + 2J'' \cos(2k_x - 2k_z). \quad (C5) \end{aligned}$$

For $J'' = 0$, it is shown that the system becomes an AI topological insulator for $-2J' < m < J'$ ⁵⁵. As shown in Fig. 12, in the AI topological insulator, the zeros of the Green functions cross in the bandgap.

- ¹ A. A. Abrikosov, L. P. Gorkov, and I. E. Dzyaloshinski, *Methods of Quantum Field Theory in Statistical Physics* (Dover, New York) (1975).
- ² A. L. Fetter and J. D. Walecka, *Quantum theory of many-particle systems* (Dover, New York) (2012).
- ³ I. Dzyaloshinskii, *Phys. Rev. B* **68**, 085113 (2003).
- ⁴ K. Seki and S. Yunoki, *Phys. Rev. B* **96**, 085124 (2017).
- ⁵ S. Sakai, Y. Motome, and M. Imada, *Phys. Rev. B* **82**, 134505 (2010).
- ⁶ Y. Yamaji and M. Imada, *Phys. Rev. B* **83**, 214522 (2011).
- ⁷ C. L. Kane and E. J. Mele, *Phys. Rev. Lett.* **95**, 146802 (2005).
- ⁸ M. Z. Hasan and C. L. Kane, *Rev. Mod. Phys.* **82**, 3045 (2010).
- ⁹ X.-L. Qi and S.-C. Zhang, *Rev. Mod. Phys.* **83**, 1057 (2011).
- ¹⁰ Y. Ando, *Journal of the Physical Society of Japan* **82**, 102001 (2013).
- ¹¹ C.-K. Chiu, J. C. Y. Teo, A. P. Schnyder, and S. Ryu, *Reviews of Modern Physics* **88**, 035005 (2016).
- ¹² S. Ryu, A. P. Schnyder, A. Furusaki, and A. W. Ludwig, *New Journal of Physics* **12**, 065010 (2010).
- ¹³ A. Kitaev, in *AIP conference proceedings* (American Institute of Physics, 2009), vol. 1134, pp. 22–30.
- ¹⁴ A. M. Essin and V. Gurarie, *Phys. Rev. B* **84**, 125132 (2011).
- ¹⁵ L. Fu and C. L. Kane, *Phys. Rev. B* **76**, 045302 (2007).
- ¹⁶ H. C. Po, A. Vishwanath, and H. Watanabe, *Nature Communications* **8**, 1 (2017).
- ¹⁷ F. Tang, H. C. Po, A. Vishwanath, and X. Wan, *Nature Physics* **15**, 470 (2019).
- ¹⁸ T. Zhang, Y. Jiang, Z. Song, H. Huang, Y. He, Z. Fang, H. Weng, and C. Fang, *Nature* **566**, 475 (2019).
- ¹⁹ F. Tang, H. C. Po, A. Vishwanath, and X. Wan, *Nature* **566**, 486 (2019).
- ²⁰ M. Vergniory, L. Elcoro, C. Felser, N. Regnault, B. A. Bernevig, and Z. Wang, *Nature* **566**, 480 (2019).
- ²¹ F. Tang, H. C. Po, A. Vishwanath, and X. Wan, *Science Advances* **5**, eaau8725 (2019).
- ²² Y. Xu, L. Elcoro, Z.-D. Song, B. J. Wieder, M. Vergniory, N. Regnault, Y. Chen, C. Felser, and B. A. Bernevig, *Nature* **586**, 702 (2020).
- ²³ P. B. Denton, S. J. Parke, T. Tao, and X. Zhang, *arXiv:1908.03795* (2009).
- ²⁴ Y. Hatsugai, *Phys. Rev. B* **48**, 11851 (1993).
- ²⁵ W. A. Benalcazar, B. A. Bernevig, and T. L. Hughes, *Science* **357**, 61 (2017).
- ²⁶ F. Schindler, A. M. Cook, M. G. Vergniory, Z. Wang, S. S. Parkin, B. A. Bernevig, and T. Neupert, *Science Advances* **4**, eaat0346 (2018).
- ²⁷ V. Gurarie, *Phys. Rev. B* **83**, 085426 (2011).
- ²⁸ Z. Wang and S.-C. Zhang, *Physical Review X* **2**, 031008 (2012).
- ²⁹ Z. Wang and B. Yan, *Journal of Physics: Condensed Matter* **25**, 155601 (2013).
- ³⁰ J. H. Wilkinson, *Rounding errors in algebraic processes*. Prentice-Hall, Inc., Englewood Cliffs, N.J. (1963).
- ³¹ S.-G. Hwang, *The American Mathematical Monthly* **111**, 157 (2004).
- ³² F. D. M. Haldane, *Phys. Rev. Lett.* **61**, 2015 (1988).
- ³³ K. Ohgushi, S. Murakami, and N. Nagaosa, *Phys. Rev. B* **62**, R6065 (2000).
- ³⁴ C.-X. Liu, X.-L. Qi, H.-J. Zhang, X. Dai, Z. Fang, and S.-C. Zhang, *Physical Review B* **82**, 045122 (2010).
- ³⁵ W. P. Su, J. R. Schrieffer, and A. J. Heeger, *Phys. Rev. Lett.* **42**, 1698 (1979).
- ³⁶ C. G. Velasco and B. Paredes, *Phys. Rev. Lett.* **119**, 115301 (2017).
- ³⁷ Z.-X. Liu, Z.-H. Li, and A.-M. Wang, *Journal of Physics: Condensed Matter* **31**, 125402 (2019).
- ³⁸ L. Fu, C. L. Kane, and E. J. Mele, *Phys. Rev. Lett.* **98**, 106803 (2007).

- ³⁹ L. Fu and C. L. Kane, Phys. Rev. B **76**, 045302 (2007).
- ⁴⁰ A. M. Turner, Y. Zhang, and A. Vishwanath, Phys. Rev. B **82**, 241102(R) (2010).
- ⁴¹ A. Matsugatani and H. Watanabe, Phys. Rev. B **98**, 205129 (2018).
- ⁴² C. Fang and L. Fu, Science Advances **5**, eaat2374 (2019).
- ⁴³ <http://www.physics.rutgers.edu/pythtb/>.
- ⁴⁴ R. Shindou and N. Nagaosa, Phys. Rev. Lett. **87**, 116801 (2001).
- ⁴⁵ S. Murakami, New Journal of Physics **9**, 356 (2007).
- ⁴⁶ X. Wan, A. M. Turner, A. Vishwanath, and S. Y. Savrasov, Phys. Rev. B **83**, 205101 (2011).
- ⁴⁷ A. Burkov, Ann. Rev. Cond. Mat. Phys. **9**, 359 (2018).
- ⁴⁸ Z. Wang, Y. Sun, X.-Q. Chen, C. Franchini, G. Xu, H. Weng, X. Dai, and Z. Fang, Physical Review B **85**, 195320 (2012).
- ⁴⁹ T. Morimoto and A. Furusaki, Phys. Rev. B **89**, 235127 (2014).
- ⁵⁰ B.-J. Yang and N. Nagaosa, Nature Communications **5**, 4898 (2014).
- ⁵¹ J. Li, R.-L. Chu, J. K. Jain, and S.-Q. Shen, Phys. Rev. Lett. **102**, 136806 (2009).
- ⁵² K. Kobayashi, T. Ohtsuki, and K.-I. Imura, Phys. Rev. Lett. **110**, 236803 (2013).
- ⁵³ L. Wang, H. Jiang, X. Dai, and X. C. Xie, Phys. Rev. B **85**, 235135 (2012).
- ⁵⁴ W. Witczak-Krempa, G. Chen, Y. B. Kim, and L. Balents, Annual Review of Condensed Matter Physics **5**, 57 (2014).
- ⁵⁵ H. M. Price, arXiv:1806.5263 (2018).
- ⁵⁶ Y. Wang, H. M. Price, B. Zhang, and Y. Chong, Nature Communications **11**, 1 (2020).